Energy Reports 6 (2020) 325–335

Contents lists available at ScienceDirect

Energy Reports

journal homepage: www.elsevier.com/locate/egyr

Research paper

Multi-objective optimization for the proper selection of the best heat pump technology in a fuel cell-heat pump micro-CHP system

Xiaochao Fan [a], Hexu Sun [a,*], Zhi Yuan [b], Zheng Li [a], Ruijing Shi [a], Navid Razmjooy [c]

[a] College of Electrical Engineering, Hebei University of Science and Technology, Shijiazhuang, Hebei, 050091, China
[b] Engineering Research Center of Renewable Energy Power Generation and Grid-connected Control, Ministry of Education, Xinjiang University, Urumqi, Xinjiang, 830047, China
[c] Department of Engineering, Tafresh University, Tafresh, Iran

ARTICLE INFO

Article history:
Received 14 December 2019
Received in revised form 15 January 2020
Accepted 27 January 2020
Available online xxxx

Keywords:
Fuel cell
Micro CHP
Heat pump
Multi-objective optimization
Sunflower optimization algorithm

ABSTRACT

In this paper, a new multi-objective technique has been proposed for optimal analysis of three different candidate heat pump solutions including the vapor compression cycle (VCC), trans-critical R744 cycle, and Peltier device to determine which one gives the best configuration and better performance on a hybrid heat pump and fuel cell-based micro-CHP system. Here, a sunflower optimization algorithm is utilized to provide two different objectives: minimizing the combined yearly maintenance and capital costs and maximizing the performance of the hydrogen energy consumption. Simulation results show that using the VCC, according to its efficient and low-cost characteristics for cell stack and lithium battery maintenance, gives the best solution for the presented hybrid system.

1. Introduction

Nowadays, energy has been turned into one of the most strategic need for the humankind such that its supply has become to a most pressing concern in the world (Infield and Freris, 2020). Looking at the depleting status of fossil energy sources on the one hand and the detrimental effects of this type of energy on the environment, on the other hand, determine the importance and necessity of optimizing energy production methods and converting fossil fuels (Tian et al., 2019; Bagal et al., 2018; Eskandari Nasab et al., 2014; Ahmadi et al., 2016a). Electricity, as one of the most important parts of energy, has a great impact on the energy basket of every country, and a large amount of it is supplied worldwide through the conversion of fossil fuels (Hosseini et al., 2011, 2012). Therefore, due to the limitation of fossil fuel resources, the issue of controlling energy costs, reducing the effects of conversion and energy consumption on the environment, reducing waste and improving the efficiency of thermal power generation is of high importance (Cao et al., 2019; Ghadimi and Firouz, 2015; Ghadimi and Ojaroudi, 2014; Ahmadi et al., 2016b).

Electricity generation coupled with the use of heat generation is a rapidly developing method that increases efficiency and reduces overall losses (Sahraie et al., 2015; Ahmadi et al., 2015). This is generally referred to as a Combined Heat and Power source (CHP) system. CHP technologies have reduced environmental emissions in the building sector and are now widely used. The CHP can potentially improve energy supply security and supply system reliability. On the other hand, CHP is a versatile technology, capable of supplying electricity and heat. The CHP systems come in a variety of sizes, from large ones used to generate electricity and heat of a city to small units that can serve a home. The new CHP boundary is in small residential buildings (Ahmadi et al., 2017). Many manufacturers are developing Micro-CHP (mCHP). These small power plants have electrical power of 1 to 15 kW and recovered the heat of 1 to 20 kW. These generators use various technologies as energy converters. Fuel cells are new technologies that can be utilized in mCHP systems. The fuel cell directly generates electrical energy from chemical energy and its efficiency is much higher than that of internal combustion engines (Mascuch et al., 2020). All components of fixed fuel cells and cells have no moving parts. The lack of moving parts makes the fuel cell work quietly (Ronaszegi et al., 2020; Mehrfeld et al., 2020). Their durability and reliability are also high, and pollutants such as nitrogen oxides and sulfur oxides are close to zero in the fuel cell. Potential fuel cells have a higher energy density than batteries and can be fed quickly and easily. Therefore, the use of fuel cells in these systems can be very significant (Yu et al., 2020).

Nonetheless, the design of a fuel cell-based micro-CHP (FC-mCHP) system is a complicated problem due to the several parameters of the system that impact its efficiency such as the energy management strategy (EMS) and component sizing to

* Corresponding author.
E-mail address: hust2019shx@126.com (H. Sun).

https://doi.org/10.1016/j.egyr.2020.01.009

achieve the minimum real-time energy consumption. Several research works have been performed for solving this problem (Liu et al., 2016; Rosli et al., 2017). Chang et al. (2017) presented a hybrid residential FC-mCHP and solar energy. The system generally contained three subsystems including PEMFC, organic Rankine cycle/domestic hot water (ORC-DHW), and vapor compression cycle (VCC). The performance of the Hybrid CCHP system was studied both in winter and in summer. The final results declared that the average performance of the system in winter and summer are 85.0% and 75.4%, respectively.

Bornapour et al. (2017) presented optimal scheduling for a hybrid PEMFC-mCHP, photovoltaic (PV), and wind turbines (WT) with considering uncertainties. A developed firefly algorithm was utilized to solve the optimization problem by considering the uncertainties in solar radiation, wind speed, and electricity market price. The optimization process is performed by considering the average energy not supplied (AENS), emission, and profit maximization as cost functions.

Romdhane et al. (2018) investigated the efficiency of an eco-neighborhood PEMFC-mCHP in France. The study modeled the overall system and validated the model base on empirical data. Then, the impact of various input parameters like relative current and humidity density and the PEMFC input pressure on micro-CHP was studied. The analysis was performed by calculating two operational strategies for two scenarios: the first scenario was about a residential house including a micro-CHP system along with a 1 kW PEMFC stack, and the second scenario includes a micro-CHP system based on a 5 kW coupled PEMFC stack with three groups of houses. The final results were analyzed and were compared with the traditional system based on gas-fired boiler connected to the grid to show the system efficiency.

Adam et al. (2018) introduced a model for the integration of a PEMFC micro-CHP system for a residential building. To achieve an optimal model for designing the PEMFC fuel cell micro-CHP systems, MINLP (mixed-integer non-linear programming model) was utilized. Dwelling's energy demand was considered to generate more general results to optimize the micro-CHP unit and the total system. The study also showed that heat emitter temperature constraints have a direct impact on the optimum design and operation of the system.

The main idea in this study is to present a new optimization technique to do a multi-objective comparative analysis on different candidate heat pump technologies to select the best configuration for a fuel cell micro-CHP. The objectives of optimization are to maximize the efficiency of the hydrogen energy consumption and to minimize the economic cost of the system. The overall novelties of the proposed method are detailed below:

- Using multi-objective optimization for analyzing the FC-CHP System.
- Using sunflower optimization algorithm for solving the optimization problem.
- Selecting an optimal selection of the heat pump configuration in a hybrid FC-CHP system
- Using system cost and also primary energy consumption efficiency for the system optimization.
- Analysis of all the heat pumps independently based on applying them into the FC-CHP system.

In the following, Section 2 illustrates the overall structure of the study, Section 3 talks about mathematical modeling of different components of the system, Section 4 represents the system efficiency calculation and validation of the model, Section 5 is about the analyzing the proposed model, Section 6 describes the final simulation results and discussions and the paper has been concluded in Section 6.

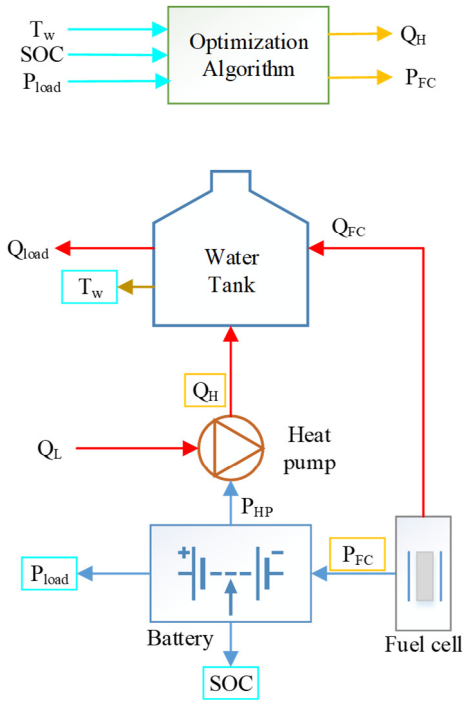

Fig. 1. The block diagram of the studied fuel cell-based micro-CHP system.

2. The system overview

The proposed system includes a configuration including the PEMFC based micro combined heating and power source. Here, the water tank absorbs its required heat from the electrochemical waste heat of fuel cell (FC) stack and the heat pump (HP), cooperatively. For improving the sustainability guaranteeing, the water tank and electric battery have been employed as thermal and electrical energy storage components, respectively. Where, the water tank and the electric battery compensate the heat rate and the power consumption (generation) differences, respectively among the power load (P_{Load}), HP, and FC stack. Fig. 1 represents the block diagram of the presented fuel cell-based micro-CHP system.

Fig. 1 shows that the heat value for all the components, such as Q_L, Q_H, and Q_{FC} can be negative or positive values as the components can be heated up or cooled down. An optimization technique is then performed to minimize the hydrogen energy consumption and also to the energy balance of the micro-CHP system. This is done by tuning the HP output heat Q_H and FC stack operating power P_{FC} for controlling the water tank temperature and battery state of charge (SOC) against the desired reference values. The demand load (P_{Load}) is considered for developing the P_{FC} response toward the scenarios including large P_{Load} values. Fig. 2 shows the model of the thermoelectric component.

In the following, the detailed equations of the system have been proposed.

3. The system modeling

In this section, the mathematical modeling of the system components has been described. Before starting the modeling, for simplifying the models, some assumptions have been considered as follows:

- The water temperature in the storage tank is assumed to be equal by the hot side temperature of the HP device.

- The temperature of the water in the ambient environment is considered equal by the cold side temperature of the HP device.
- The wasted heat derived from FC stack walls, water tank walls, and pipe connections has been neglected in the simulations.
- The impact of a conditional liquid cooling circuit to interface the HP device, water tank, and the FC stack together is neglected.
- The thermal waste heat in the compressor wall has been neglected (Nawaz et al., 2018).
- The only loss in the compressor for the trans-critical R744 cycle or vapor compression cycle which has been accounted for the modeling is isentropic efficiency (Wang et al., 2018b).
- Power electronic devices' losses have been neglected.

3.1. The mathematical model of the fuel cell

The principal model of the output voltage of a single fuel cell is mentioned as follows (Haghighi and Sharifhassan, 2016; Corrêa et al., 2004; Aouali et al., 2017):

$$V_{out} = N_{nc}\left(E_{oc} - E_{act} - E_{\Omega} - E_{ops}\right) \tag{1}$$

where, N_{nc} determines the number of FC stack cells which are connected in series, E_{act} describes the activation polarization loss, E_{oc} represents the open circuit potential condition per cell, E_{Ω} is the Ohmic voltage drop in the cells, and E_{ops} represents the over-potential saturation in the cells (Aghajani and Ghadimi, 2018; Liu et al., 2017).

In the above equation, the open-circuit voltage of the fuel cell stack is in standard temperature (25 °C) and pressure (1 atm) is obtained as follows (Gollou et al., 2017):

$$E_{oc} = 1.3 - 85 \times 10^{-5}\left(T_{PEM} - 298.15\right) + 4.31 \times 10^{-5} \times T_{PEM} \times ln\left(P_{H_2}\sqrt{P_{O_2}}\right) \tag{2}$$

where,

$$P_{O_2} = P_c \times e^{-\left(\frac{1.635 I_{PEM}/A}{T^{1.334} I_{PEM}}\right)} - \left[R_{hc} \times P_{H_2O}\right]^2 \tag{3}$$

$$P_{H_2} = 0.5 \times P_a \times e^{-\left(\frac{1.635 I_{PEM}/A}{T^{1.334} I_{PEM}}\right)} - \left[R_{ha} \times P_{H_2O}\right]^2 \tag{4}$$

$$\log_{10}\left(P_{H_2O}\right) = 0.03 \times \left(T_{PEM} - 273.15\right) - 9.18 \times 10^{-5} T_c^2 + 1.4 \times 10^{-7} T_c^3 - 2.18 \tag{5}$$

The optimal mathematical model for the activation over-potential is as follows (Cao et al., 2019):

$$E_{act} = -\left[-0.89 + 3.42 \times 10^{-3} \times T_{PEM} + 7.76 \times 10^{-5} \times T_{PEM} \ln\left(C_{O_2}\right) - 9.55 \times 10^{-5} \times T_{PEM} \ln\left(I_{PEM}\right)\right] \tag{6}$$

where, C_{O_2} represents the saturation value of the O_2 in the catalytic (mol/cm^3) and is modeled as follows:

$$C_{O_2} = 2 \times P_{O_2} \times 10^{-7} \times e^{\frac{498}{T_{PEM}}} \tag{7}$$

And the saturation value of the H_2 in the catalytic interface (mol/cm^3) is modeled as follows:

$$C_{H_2} = 9 \times P_{H_2} \times 10^{-7} \times e^{\frac{-77}{T_{PEM}}} \tag{8}$$

The Ohmic voltage drop of the cells is obtained as follows:

$$E_{\Omega} = I_{PEM} \times \left(R_m + R_{hc}\right) \tag{9}$$

where (Wang et al., 2018b),

$$R_m = l \times \rho_m \times S^{-1} \tag{10}$$

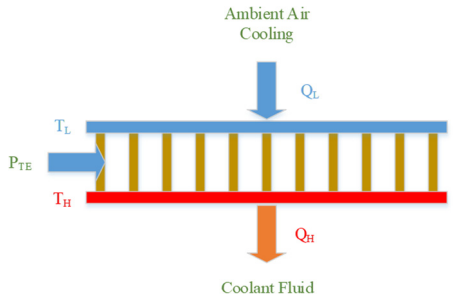

Fig. 2. The general model of a thermoelectric device.

$$\rho_m = \frac{181.6 \times \left[0.062\left(\frac{T_{PEM}}{303}\right)^2\left(\frac{I_{PEM}}{S}\right)^{2.5} + 0.03\left(\frac{I_{PEM}}{S}\right) + 1\right] \times e^{-\left(\frac{T_{PEM}-303}{I_{PEM}}\right)}}{\left[13 - 0.063 - 3\left(\frac{I_{PEM}}{S}\right)\right]} \tag{11}$$

And the optimal value for the over-potential saturation (E_{ops}) in the cells based on (Wang et al., 2018b) is as follows:

$$E_{ops} = 0.05 \times ln\left(\frac{J}{J_{max}} - 1\right) \tag{12}$$

where, T_{PEM} represents the operating cell temperature, I_{PEM} represents the operating current of the fuel cell, S represents the area of the membrane, P_{O_2}, P_H, and P_{H_2O} is the partial pressure of the O_2, H_2, and H_2O, respectively, P_c and P_a are the inlet pressure for the cathode and the anode, R_{hc} and R_{ha} are the relative humidity of the vapor at cathode and anode, respectively, C_{H2} and C_{O2} describes the saturation of the H_2 and O_2 (mol/cm^3), R_c and R_m describe the connections resistance and the membrane resistance, I is the membrane thickness, ρ_m determines the membrane resistivity, J is the density of the real current, and J_{max} represents the maximum value of J.

Therefore, the operating electrochemical performance is determined as follows:

$$\eta_{FC} = \frac{0.67 \times V_{out}}{N_{nc} \times E} \tag{13}$$

where, E is the instantaneous stored energy.

Finally, the produced waste heat is achieved as follows:

$$Q_{FC} = P_{FC}\left(\frac{1}{\eta_{FC}} - 1\right) \tag{14}$$

All the thermodynamic characteristics of the studied PEMFC are extracted from Wang et al. (2018b).

3.2. The model of heat pump device

The heat pump in this study contains three main parts including the Peltier device, trans-critical R744 cycle, and vapor compression cycle. In the following, the mathematical model of the components has been explained.

(A) model of a Peltier device

By assuming the steady-state conditions, the portion of the energy flow in a unit associated with thermoelectric devices is formulated as follows (Mirzapour et al., 2019):

$$T \times J \times \frac{d\alpha}{dx} + \tau \times J \times \frac{dT}{dx} - \rho \times J^2 - \frac{d}{dx}\left(k \times \frac{dT}{dx}\right) = 0 \tag{15}$$

where, J represents the density of the electric current, T describes the absolute temperature, τ describes the Thomson coefficient, α defines the coefficient of the Seebeck, k is the material thermal conductivity, and ρ describes the electrical resistivity.

Table 1
The features of TEC1-12712 Firouz et al. (2016).

Parameter	Value	Unit
Rated power (W)	118	W
Number of thermocouples	126	–
The length of thermocouple (l)	1.9	mm
Cover plate area	5 × 5	cm^2
Area of the thermocouples (A)	1.4 × 1.4	mm^2

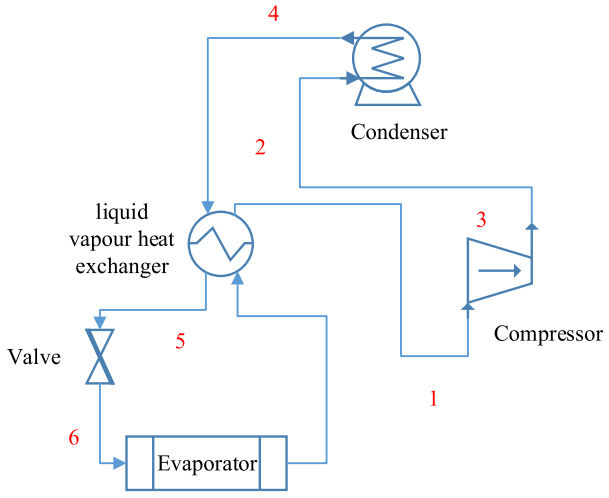

Fig. 3. The schematic of the vapor compression refrigeration cycle.

Consider the thermoelectric device with a couple of two antithetic semiconductors by assuming averaged transport characteristics. Then, for the N arm:

$$k_N \frac{d^2T}{dx^2} - \tau_N \times J \times \frac{dT}{dx} + \rho_N \times J^2 = 0 \tag{16}$$

where, the index N shows the averaged characteristics.

By considering the reverse direction of the current, the above formulation can be extended to the P arm. The heat flow at the junction of two opposite conductors at the hot side and cold side are as follows:

$$Q_h = \alpha \times T_h \times I - 0.5 \times \tau_m \times I \times \Delta T + 0.5 \times I^2 \times R_m - K_m \times \Delta T \tag{17}$$

$$Q_c = \alpha \times T_c \times I + 0.5 \times \tau_m \times I \times \Delta T - 0.5 \times I^2 \times R_m - K_m \times \Delta T \tag{18}$$

where, the index m shows the averaged characteristics.

In this condition, the electrical power is formulated as follows:

$$P_e = Q_h - Q_c = \alpha \times (T_h - T_c) \times I - \tau_m \times I \times \Delta T + I^2 \times R_m \tag{19}$$

And the voltage of the thermoelectric terminals is as follows:

$$V_p = \alpha \times (T_h - T_c) + I \times R_m \tag{20}$$

The model of the studied Peltier Module here is TEC1-12712. Table 1 illustrates the features of this module in the study

(B) Model of a vapor compression cycle

By assuming the steady-state cyclic operation and the cycle diagram of vapor compressor refrigeration in Fig. 3, the T–S and P–S cycle diagram is presented in Fig. 4(a) and (b), respectively

Based on Fig. 3 and the thermodynamics first law with the fact that the internal energy variation is zero for a cyclic process,

$$Q_{Co} + Q_{co}^{loss} - \left(Q_{ev} + Q_{ev}^{loss}\right) - \left(W + Q_W^{loss}\right) = 0 \tag{21}$$

where, Q_{Co} describes the condenser heat rejection ratio (kW), Q_{co}^{loss} represents the hot refrigerant heat leak ratio (kW), Q_{ev} describes the absorbed heat by the evaporator ratio (kW), Q_{ev}^{loss} is the heat leak ratio from the ambient to the cold refrigerant (kW), W represents the compressor input power (kW) and Q_W^{loss} describes the compressor shell to ambient heat leak ratio (kW).

The required electrical energy for the compressor is achieved as follows (Hamian et al., 2018):

$$W = m_r\,(h_5 - h_4) \tag{22}$$

where, m_r describes the refrigerant mass flow rate.

The rate of heat absorbed by the evaporator can be formulated as follows (Hamian et al., 2018):

$$Q_{ev} = (\varepsilon \times C)_{ev} \times \left(T_{ev}^{in} - T_{ev}\right) = m_r \times (h_2 - h_3) \tag{23}$$

where, C represents the external fluids capacitance ratio, ε describes the impact of the heat exchanger, T_{ev}^{in} describes the inlet temperature of the evaporator coolant, h describes the specific enthalpy of the refrigerant at state point, T_{ev} describes the evaporator refrigerant temperature.

Similarly, for the condenser, we have:

$$Q_{Co} = (\epsilon \times C)_{co} \times \left(T_{co}^{in} - T_{co}^{loss}\right) = m_r \times (h_6 - h_1) \tag{24}$$

where, T_{co} describes the refrigerant temperature in the condenser and T_{co}^{in} represents the condenser coolant inlet temperature.

The COP in this condition can be considered as the refrigerating impact on the network input as follows:

$$COP = Q_{ev}/W \tag{25}$$

(C) Model of a trans-critical R744 cycle

R744 (carbon dioxide) is one of the environment-friendly solutions to prevent the high effects of the typical refrigerants which are employed as natural refrigerants (Leng et al., 2018). To make sure that a suitable comparison including the same thermodynamic conditions is obtained between the vapor compression cycle and the R744 cycle which contains the setting of the condenser and evaporator outlet temperatures (T3 and T1) to equal the stored water temperature by the ambient temperature, respectively.

Nevertheless, the concept of the trans-critical R744 cycle represents that various thermodynamic impacts are included and a developed mathematical model is important. In addition, based on the Ref. Nawaz et al. (2018), trans-critical R744 cycles give an optimal COP according to the conditions at the condenser and evaporator. The pressure of discharge in the optimal compressor is related to the cycle of the highest temperature. That is why the term S_H is introduced here to determine the degree to which T_3 (the temperature at point 2) is greater than T_4 (upstream of the evaporator):

$$T_3 = S_H \times T_4 \tag{26}$$

where, $S_H > 1$ to satisfy the $T_3 > T_4$ requirement.

After evaluating the enthalpy of all points in the trans-critical R744 cycle, required compressor power, the appropriate R744 mass flow rate, and total heat absorbed by the evaporator are given in Eqs. (22), (23) and (25).

(D) Model for electric heating

Electric heating is the process of generating heat energy from electrical energy. The electrical resistor is the main component of the heating element inside every electric heater. This process is performed based on the principle of Joule heating. Alternatively, the heat pump utilizes an electric motor to do the refrigeration cycle which draws heat energy from the original source and transforms the generated heat to the required place. By neglecting the heat loss, the heat generation (Q_H) is equal to

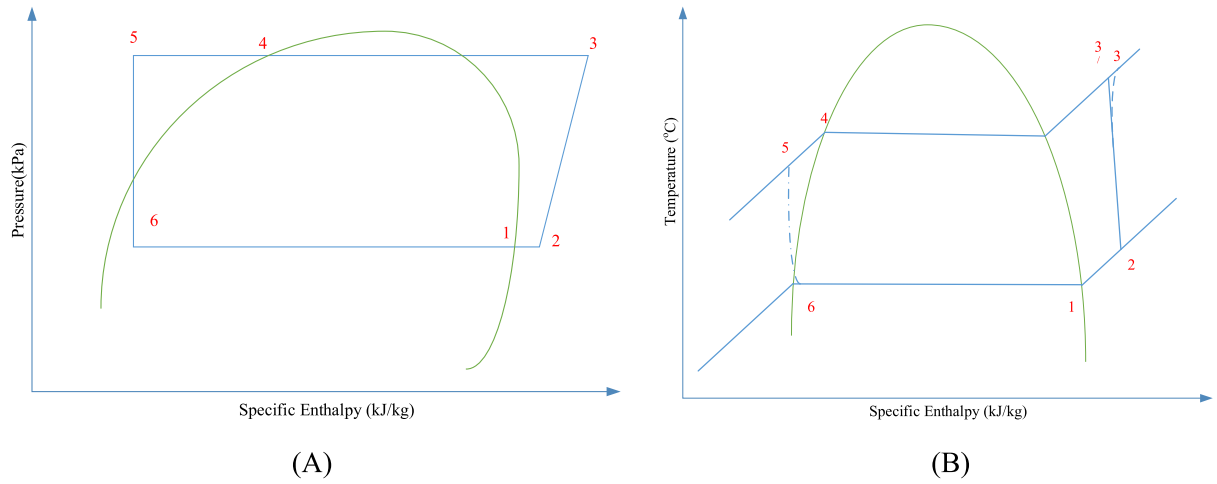

Fig. 4. A simple example of the thermodynamic cycle on (A) pressure-specific enthalpy and (B) temperature-specific enthalpy diagram for R134a fluid.

the consumption value of the electric heater's electricity (P_{HP}). In this condition, by assuming the ambient sourced heat as zero ($Q_L = 0$), in accordance with the electric heating method, the heat pump has been effectively replaced in the FC-mCHP system. In this study, the power of electric heating required in the system is provided by the battery and fuel cell. The operating electric heater here is equivalent to a heat pump that has a heating COP equal to 1 and a cooling COP equal to 0.

3.3. The mathematical model of the electric battery

Electric batteries are a set of one or more cells that generate chemical reactions of electrons in a circuit. These components are modeled as kinds of energy storage devices which contain a specified value of maximum storage capacity (E_{Max}) and stored energy, E. The total power flows in and out of battery are dynamically used for changing the stored energy. The power of the battery based on Fig. 1 is formulated below (Akbary et al., 2019):

$$\frac{dE}{dt} = P_{FC} + P_{HP} - P_{Load} \tag{27}$$

where, P_{Load} describes the demanded electric power from the user.

And the SOC of the battery based on (Akbary et al., 2019) is as follows:

$$SOC = \frac{E}{E_{Max}} \tag{28}$$

3.4. The method of EMS

The EMS (Energy management strategy) is an algorithm for ensuring a balanced energy level in the storage elements alongside applying a real-time controlling for the Q_H and P_{FC} toward the user's energy demands satisfaction. Here, Q_H is calculated as a function of battery SOC and P_{FC} is calculated as a function of the fuel cell temperature. The pseudo-code of the control configuration for selecting the amount of Q_H and P_{FC} is given below (Akbary et al., 2019) (see Fig. 5):
where,

$$m = \frac{P_{FC\_max} - P_{FC\_min}}{SOC_{min} - SOC_{max}} \tag{29}$$

Therefore, based on the above figure, there are two main purposes: the purpose of the Q_H is to keep the stored water temperature (T_w) close to the desired reference range. In addition, the objective of the P_{FC} is to keep the battery in its SOC limitations. At last, the value of the P_{HP} is achieved based on the reference Q_H value.

4. System performance evaluation and validation

Hydrogen Energy can be transformed into free electricity with the help of Fuel Cell technology. Hydrogen is always known as a perfect fuel. There is a large amount of hydrogen in the ground (for example in water) and can be used as fuel. Burning hydrogen is not only harmful but also quite beneficial to nature. Hydrogen never runs out. However, hydrogen is not primary energy such as oil or coal. But like electricity, it is a carrier of clean energy. Hydrogen is very suitable for long-distance storage and transport. Creating transmission lines, of course, is quite expensive and costly.

In this study, for the analysis of the studied FC-mCHP, the efficiency of hydrogen energy consumption has been provided. This indicator shows the proportion of the total energy consumption and the total energy stored by the system toward the total energy that is stored internally in the consumed hydrogen fuel. Therefore, the efficiency of hydrogen energy consumption is achieved as follows:

$$\eta_{H2} = \frac{\int_0^{t_e} (P_{Load} + Q_{Load})\,dt + Co_w C_{p(w)} (T(t_e) - T(0)) + E_{Max} (SOC(t_e) - SOC(0))}{V_{LH} \times C_{H_2}} \tag{30}$$

where, t_e describes the end time of simulation, Co_w determines the total water consumed, $C_{p(w)}$ represents the specific heat capacity (J/ (kg K)), V_{LH} describes the lower heating value of the H_2 and is assumed 120 MJ/kg, and Co_{H_2} is the total consumed hydrogen and is as follows:

$$Co_w = \int_0^{t_e} \dot{m}_{H_2} dt \tag{31}$$

Another indicator that is utilized here for the FC-mCHP system improvement is the economic cost of the system. To do so, in this study, the ongoing maintenance cost (C_M) and the initial capital cost (C_i) have been employed, i.e. the total economic cost is:

$$C_T = \sum (C_M + C_i) \tag{32}$$

where,

$$C_i = C_u \tag{33}$$

$$C_M = C_i / C_y \tag{34}$$

Start

For Q_H

if $T_w < T_{r\_min}$ $Q_H = 1000 + Q_{Load} - Q_{FC}$

else if $T_w > T_{r\_max}$ $Q_H = -Q_{FC}$

else $Q_H[q+1] = Q_H[q]$

For P_{FC}

if $SOC \geq 1 \rightarrow P_{FC}[q+1] = 0$

else if $SOC \leq SOC_{min}$ *or* $P_{Load} \geq 1.5P_{FC\_max} \rightarrow P_{FC}[q+1] = P_{FC\_max}$

else if $SOC_{min} \leq SOC \leq SOC_{max} \rightarrow P_{FC}[q+1] = m(SOC - SOC_{min}) + P_{FC\_max}$

else $P_{FC}[q+1] = P_{FC}[q]$

End

Fig. 5. The pseudo-code of the control configuration for selecting the amount of Q_H and P_{FC}.

Table 2
The cost of C_u utilized in the present study.

Component	Cost (in USD)
Compressor	0.042/W
Expansion valve	0.082/W
Electric heater	0.022/W
Battery	$0.22/Wh
The heat pump (type 1)	$3.96N_{TEH}$
Fuel cell stack	$5247.11/kW

where C_u is the cost based on per unit size value and s_c describes the component size, and C_y determines the component yearly replacement cost. Table 2 illustrates the utilized C_u values used in this study. The costs of these components have been gathered from commercial websites such as Alibaba, Taobao, and eBay.

The model of parameter C_y for the components that have been achieved by the empirical results of the literature review and are given in the following.

For the heat pump, based on the (Ebrahimian et al., 2018), the air conditioning component has a lifetime of 10 years and for the thermoelectric heater, the lifetime has been assumed infinitely.

For the lithium-ion battery (Khodaei et al., 2018), the lifetime formula based on is as follows:

$$C_{y(battery)} = \frac{C_{y(battery)\_max}}{\int (1 - SOC) \times |SOC|\, dt} \tag{35}$$

where, $C_{y(battery)\_max} = 10{,}000$, and the term $(1 - SOC)$ determines the depth of discharge.

And for the fuel cell, the lifetime formula based on (Chen et al., 2015) is as follows:

$$C_{y(FC)} = \frac{\Delta V}{U_1 t_1 + U_2 t_2} \tag{36}$$

where, $U_1 = 8.7$ μV/h and $U_2 = 11$ μV/h is the rate of degradation in the best state of the fuel cell which defines the time that the fuel cell works at less than half of its rated power. $U_2 = 11$ μV/h is the rate of degradation when the fuel cell gives high power which is happened when the fuel cell operates at more than half of its rated power.

5. Model analysis

Here, the COP results of the vapor compression cycle and trans-critical R744 cycle and the models have been validated and compared with fluid R410a by Park et al. under identical thermodynamic conditions. To achieve a fair comparison with the previous work (Park et al., 2015), identical values of the variables have been extracted from Park et al. (2015) as follows:

- The condenser temperature fixed at 45.15 °C
- The temperature of the evaporator is in the range [−30 °C, 10 °C]
- The evaporator reference temperature for the heat pump fixed at 10.15 °C
- The gas cooler temperature is considered varied.

Fig. 6(A) shows the trans-critical R744 cycle validation and Fig. 6(B) shows the vapor compression cycle validation for the performed simulation and the work by Park et al. (2015).

As can be observed from Fig. 6, for both the trans-critical R744 cycle and vapor compression cycle, a clear deviation occurs in the COP results during the small temperature differential values of the condenser and evaporator (like −253.15 °C). In a reverse way, the COP converges into almost identical trends and values.

The reason for the deviation of the COP results in the lower temperature is the inaccuracy associated with the heat transfer and compressor performance effects. Nonetheless, due to using a larger condenser to evaporator temperature differences in this study, the trans-critical R744 cycle and the vapor compression cycle models can be assumed accurate for the optimization.

6. Problem statement

To the optimal analysis of the FC-mCHP system to apply the comparisons between the available heat pump technologies, a multi-objective optimization approach has been used. The optimization objective (cost function) is to minimize the cost of the total system and to maximize the energy consumption performance of the hydrogen, i.e.

$$F_1 = -\eta_{H2} \tag{37}$$
$$F_2 = C_t$$

Subject to:

$$0 \leq SOC \leq 1 \tag{38}$$
$$\max(P_{HP\_Thermo}) < P_{Thermo(Max)} \times N_{Thermo}$$

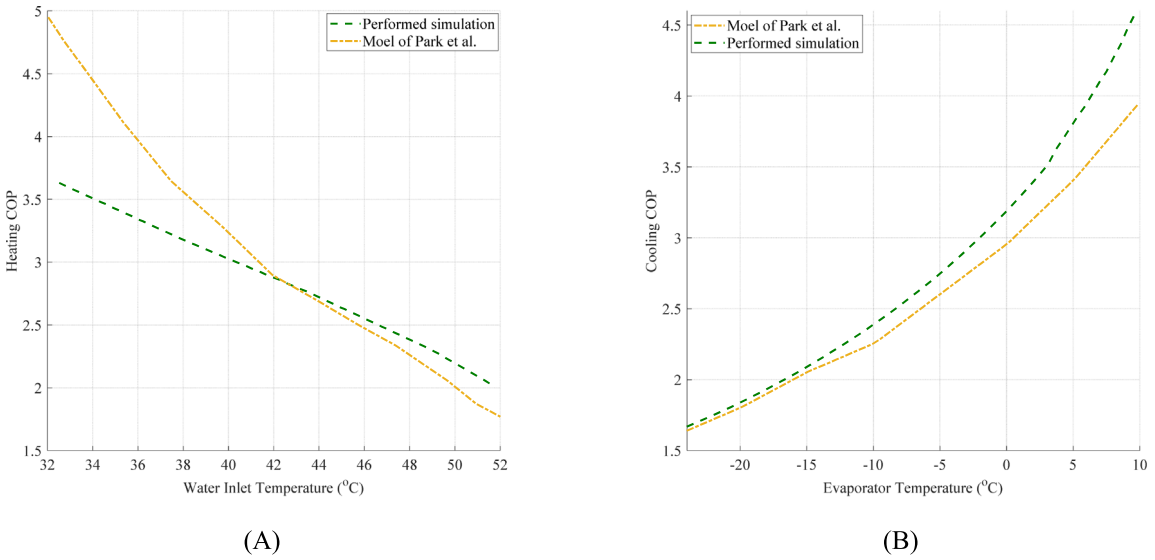

Fig. 6. The validation of the COP results for the performed simulation and Parker's method (Park et al., 2015). In (A) trans-critical R744 cycle for heating COP and (B) VCC for cooling COP.

That shows the battery SOC should be kept in the range [0, 1] during the simulation time and the second constraint declares that the rated value of the Peltier device power consumption should be more than the maximum value of it. Therefore, this constraint should be used only when the Peltier device is considered in the optimization process.

The optimization parameters include the size of the fuel stack (S_{FC}) in the range [1, 5] kW, the battery size (E_{Max}) in the range [1, 30] kWh, the number of Peltier modules in series (N_{TEH}), for only type 1 heat pumps in the range [1, 30], and finally, the specifies the studied heat pump with four types (HP_{Type}) such that type 1 defines the Peltier device, type 2 defines the CO_2 cycle, type 3 defines the VCC, and type 4 defines the electric heating, i.e. the selection search space is 1, 2, 3, and 4.

In this study, for solving the multi-objective optimization problem for the FC-mCHP, a new bio-inspired algorithm has been utilized. The range of applications, ease of use and the ability to achieve near-absolute optimal response are some of the reasons for the success of the bio-inspired algorithms (Razmjooy et al., 2016; Namadchian et al., 2016; Razmjooy and Ramezani, 2014; Ghadimi et al., 2018; Razmjooy and Ramezani, 2016; Wang et al., 2018a). These algorithms are proper solutions to multi-objective problems (Yu et al., 2019). There are several types of bio-inspired algorithms like Variance Reduction of Gaussian Distribution (VRGD) (Namadchian et al., 2016), World Cup Optimization (WCO) algorithm (Razmjooy et al., 2016), Emperor Penguin Optimizer (EPO) (Dhiman and Kumar, 2018), Owl Search Algorithm (OSA) (Jain et al., 2018), Butterfly Optimization Algorithm (BOA) (Arora and Singh, 2019), Moth Search Algorithm (Wang, 2018), Improved Cat Swarm Optimization (ICSO) algorithm (Kumar and Singh, 2018), and sunflower optimization (SFO) algorithm (Gomes et al., 2019).

In this study, the sunflower optimization algorithm has been used (Gomes et al., 2019). The SFO algorithm inspired by the special behavior of the sunflowers in seeking the best motivation toward the sun. In the SFO algorithm, the pollination can be randomly applied by considering the minimal distance between the sunflowers. Another characteristic that is considered in the algorithm is the *inverse square law radiation* which has an inversely proportional with the square of the distance and the radiation intensity.

The movement of the algorithm is to the direction to achieve more global optimum (sun) as can be possible. The obtained heat (H) from the ith the plant is as follows:

$$H_i = \frac{P_s}{4\pi d_i^2} \tag{39}$$

where, d describes the distance between a plant and the current best and P_s describes the source power.

And the movement of the sunflowers into the sun is modeled as follows:

$$\vec{D_i} = \frac{X^* - X_i}{\|X^* - X_i\|} \tag{40}$$

where, X^* and X are the best plantation and the current plantation, respectively.

The step for the sunflowers on the direction S_i is:

$$S_i = \omega \times P_i\left(\|X_i + X_{i-1}\|\right) \times \|X_i + X_{i-1}\| \tag{41}$$

where, ω describes the plants inertial displacement and P_i ($\|X_i + X_{i-1}\|$) represents the pollination probability.

The algorithm updates the closer sunflowers with smaller steps to the sun in the local updating and the other plants with farther distances move normally. The maximum step of the plants is modeled as follows:

$$S_{max} = \frac{\|X_{max} - X_{min}\|}{2 \times N_{pop}} \tag{42}$$

where, X_{max} and X_{min} represents the maximum and the minimum ranges and N_{pop} describes the plants number for all the plants. The updated plantation is achieved as follows:

$$\vec{X}_{i+1} = \vec{X}_i + S_i \times \overrightarrow{D_i} \tag{43}$$

Fig. 7 shows the method of applying the SFO algorithm to the FC-mCHP system.

7. Simulation results

Two sample examples of the optimization of the FC-mCHP system for heat pump technologies are illustrated in Table 3. The given solutions show the trade-off between the two discrete values of the cost functions such that the total population in the Pareto front includes F_1 values that change diversely in the range

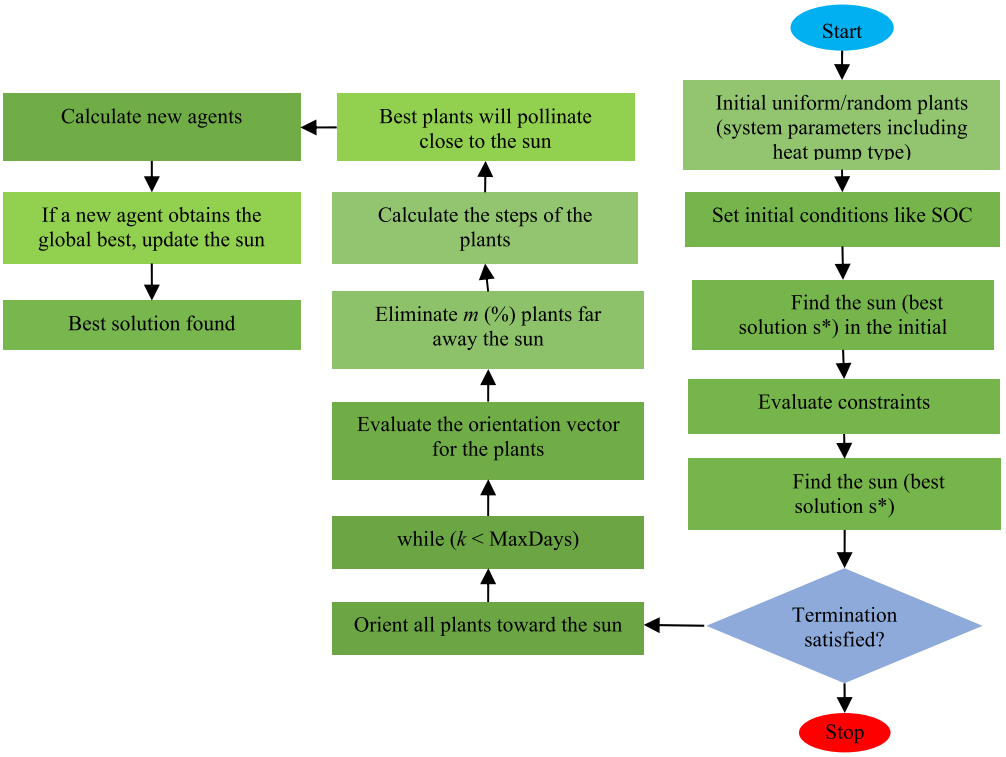

Fig. 7. The method of applying the SFO algorithm to the FC-mCHP system.

Table 3
Two sample examples of the optimization of the FC-mCHP system for heat pump technologies.

#	F_1	F_2	Battery size	Fuel cell size
1	−1.19	23 517	6115 Wh	2 kW
2	−1.72	18 308	3824 Wh	3 kW

of 1.19 to 1.72 and F_2 values that are basically placed in the range \$18308 to \$23517 with no solutions outside around them.

As can be observed from Table 3, it is concluded that the fuel cell stack contains the biggest part of the system's cost and the other components have less impact on the system objective minimization. The difference of the total system cost between two heat pump technologies is due to the fuel cell stack size selection, i.e. 2 kW and 3 kW. From Table 3, it is also clear that the size of the Pareto front for the optimization is almost small such that they give an almost unique performance for the proposed FC-mCHP configurations.

The results of the optimization can be clearer by determining the value for the battery size and the fuel cell stack. Therefore, the optimization of the system improves the system efficiency and gives a promising result to the demand load profile. Fig. 8 shows this condition.

Table 4 illustrates the cost value for the components of four case studies based on the optimal solutions of the Pareto front population. It is observed that the fuel cell stack includes a further part of the system's cost in all the cases.

Therefore, the essential determinant part of the system's total cost depends on the fuel cell stack selection. Table 4 also illustrates that to develop the 3 kW fuel cell stacks; there is a need for the batteries with higher capacitance. The results show that selecting a 2 kW fuel cell stack gives better results with lower investment costs while the performance of the hydrogen energy consumption improvement is very small. For the studied type 1

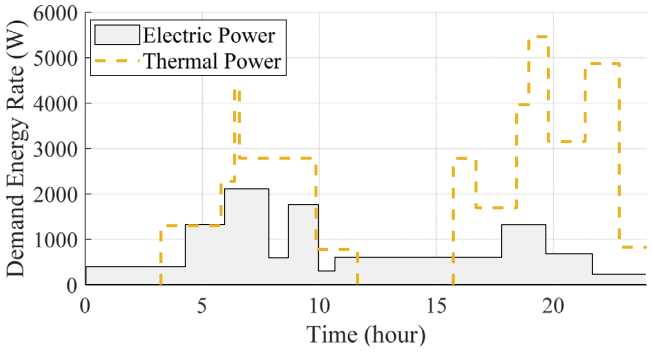

Fig. 8. General thermal and electrical load demand profile for a house on a winter day (Cao et al., 2019).

heat power, 100 numbers of solutions for the vapor compression cycle is selected. In other words, among the trans-critical CO2 cycle, Peltier device, electric heating, and vapor compression cycle, the last one is just used to achieve the objectives of the studied optimization problem. The reason behind this selection is the high-value COP of the vapor compression cycle that causes the minimum electric power consumption for the heat power operation. Fig. 9 shows the comparison of a specific solution who has its HP type varied.

As can be observed from Fig. 9, the main results are that the vapor compression cycle has the higher energy consumption performance than the Peltier and the pure electric heating. It also needs less battery capacity than the others (except VCC) as a costly component of the system.

Figs. 10 and 11 show the main transient results of different key parameters in the system. Based on Fig. 10, it is clear that the water temperature can track the reference operating range to get stabilized for most of the simulation times.

Table 4
The cost value for the components of four case studies based on the optimal solutions of the Pareto front population.

	3 kW FC, 15714 Wh battery	3 kW FC, 15626 Wh battery	2 kW FC, 8970 Wh battery	2 kW FC, 4108 Wh battery
Fuel cell stack	$28 000	$27 500	$19 000	$19 000
Battery	$3000	$2500	$2000	$1000
Heat pump	$700	$750	$500	$500

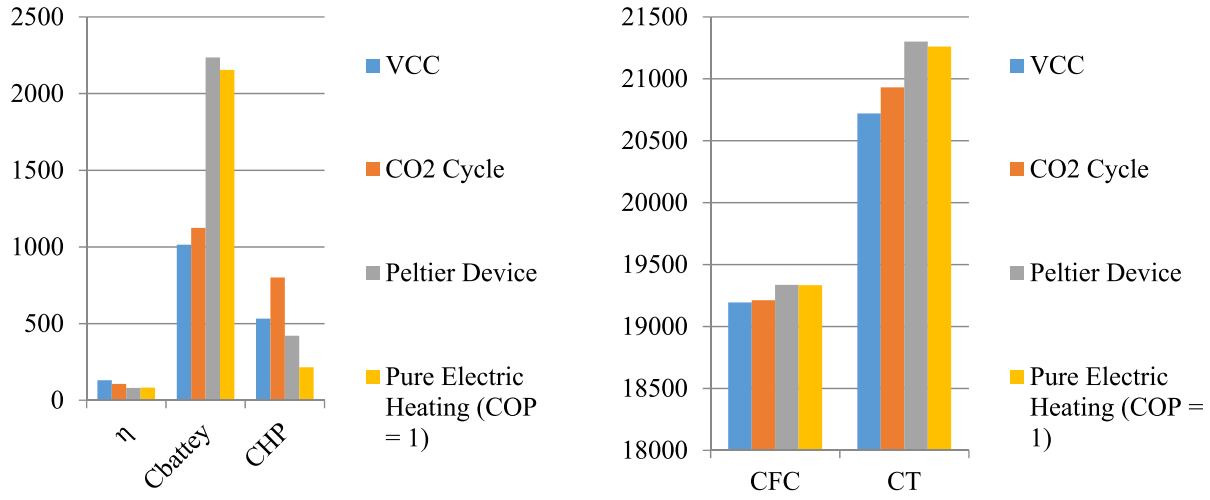

Fig. 9. The comparison of a particular solution who has its HP type varied.

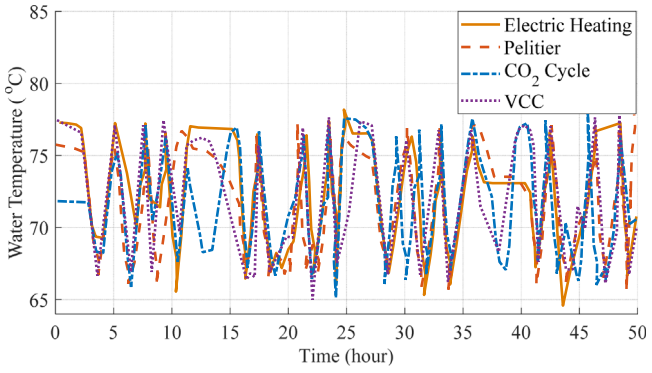

Fig. 10. Transient results of the stored water temperature.

Fig. 11 shows the substantial differences for the results of the transient of the battery SOC among the three heat pump technologies.

By giving a glance to the results of Figs. 10 and 11, it is clear that in some periods of time the values drop under zero which shows the inappropriateness of the electric heaters and the Peltier devices for feasible coupling with the selected fuel cell stack and battery sizes according to Fig. 10.

8. Conclusion

In this study, a new multi-objective optimization technique was proposed for the efficiency selection of the best model for some different heat pumps (HP) technologies over the fuel cell micro-CHP configurations. Here, three different HP technologies including vapor compression cycle, trans-critical R744 cycle, and Peltier device were used and their mathematical modeling were presented and analyzed on a residential home in the winter. The multi-objective problem here was based on two main objectives including combined yearly maintenance and capital costs minimization and hydrogen energy consumption efficiency maximization. The multi-objective optimization of the problem was applied based on a newly optimization technique, sunflower optimization (SFO) algorithm. Final results were compared with a desired VCC for showing the best configuration in the fuel cell micro-CHP system. In the future work, the model of a developed CCHP system based on solid oxide Fuel cell system will be studied to improve the system efficiency.

Declaration of competing interest

The authors declare that they have no known competing financial interests or personal relationships that could have appeared to influence the work reported in this paper.

CRediT authorship contribution statement

Xiaochao Fan: Conceptualization, Data curation, Writing - original draft, Writing - review & editing. **Hexu Sun:** Conceptualization, Data curation, Writing - original draft, Writing - review & editing. **Zhi Yuan:** Conceptualization, Data curation, Writing - original draft, Writing - review & editing. **Zheng Li:** Conceptualization, Data curation, Writing - original draft, Writing - review & editing. **Ruijing Shi:** Conceptualization, Data curation, Writing - original draft, Writing - review & editing. **Navid Razmjooy:** Conceptualization, Data curation, Writing - original draft, Writing - review & editing.

Acknowledgments

This research was funded by the National Natural Science Foundation of China, grant number Nos. 51666017, 51877070, 51577048, the Natural Science Foundation of Hebei Province of China, grant number No. E2018208155, the Talent Engineering Training Support Project of Hebei Province, grant number No. A201905008, Hebei Province Higher Education Science and Technology Research Key Project, grant number No. ZD2018228.

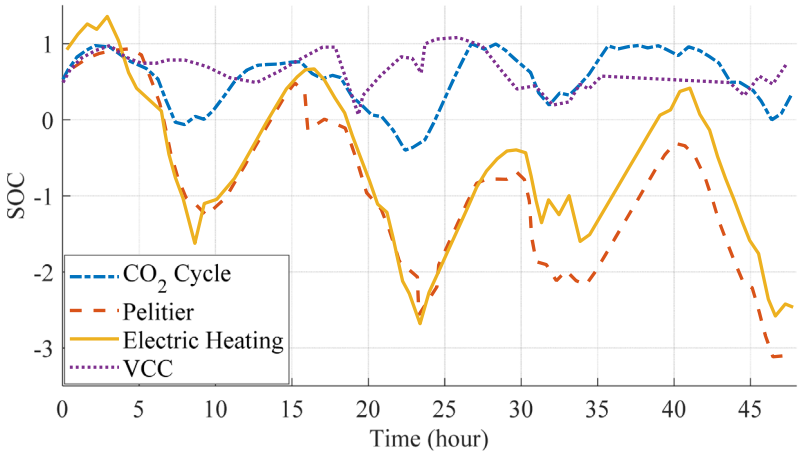

Fig. 11. Transient results of the battery SOC.

References

Adam, A., Fraga, E.S., Brett, D.J., 2018. A modelling study for the integration of a PEMFC micro-CHP in domestic building services design. Appl. Energy 225, 85–97.

Aghajani, Gholamreza, Ghadimi, Noradin, 2018. Multi-objective energy management in a micro-grid. Energy Rep. 4, 218–225.

Ahmadi, M.H., Ahmadi, M.A., Mehrpooya, M., Sameti, M., 2015. Thermo-ecological analysis and optimization performance of an irreversible three-heat-source absorption heat pump. Energy Convers. Manag. 90, 175–183.

Ahmadi, M.H., Ahmadi, M.A., Pourfayaz, F., Bidi, M., Hosseinzade, H., Feidt, M., 2016a. Optimization of powered stirling heat engine with finite speed thermodynamics. Energy Convers. Manag. 108, 96–105.

Ahmadi, M.H., Mehrpooya, M., Abbasi, S., Pourfayaz, F., Bruno, J.C., 2017. Thermo-economic analysis and multi-objective optimization of a transcritical CO2 power cycle driven by solar energy and LNG cold recovery. Therm. Sci. Eng. Prog. 4, 185–196.

Ahmadi, M.H., et al., 2016b. Thermodynamic analysis and optimization of a waste heat recovery system for proton exchange membrane fuel cell using transcritical carbon dioxide cycle and cold energy of liquefied natural gas. J. Nat. Gas Sci. Eng. 34, 428–438.

Akbary, Paria, et al., 2019. Extracting appropriate nodal marginal prices for all types of committed reserve. Comput. Econ. 53 (1), 1–26.

Aouali, F.Z., Becherif, M., Ramadan, H.S., Emziane, M., Khellaf, A., Mohammedi, K., 2017. Analytical modelling and experimental validation of proton exchange membrane electrolyser for hydrogen production. Int. J. Hydrogen Energy 42 (2), 1366–1374.

Arora, S., Singh, S., 2019. Butterfly optimization algorithm: a novel approach for global optimization. Soft Comput. 23 (3), 715–734.

Bagal, H.A., Soltanabad, Y.N., Dadjuo, M., Wakil, K., Ghadimi, N., 2018. Risk-assessment of photovoltaic-wind-battery-grid based large industrial consumer using information gap decision theory. Sol. Energy 169, 343–352.

Bornapour, M., Hooshmand, R.-A., Khodabakhshian, A., Parastegari, M., 2017. Optimal stochastic scheduling of CHP-PEMFC, WT, PV units and hydrogen storage in reconfigurable micro grids considering reliability enhancement. Energy Convers. Manag. 150, 725–741.

Cao, Y., Li, Y., Zhang, G., Jermsittiparsert, K., Razmjooy, N., 2019. Experimental modeling of PEM fuel cells using a new improved seagull optimization algorithm. Energy Rep. 5, 1616–1625.

Chang, H., et al., 2017. Energy analysis of a hybrid PEMFC–solar energy residential micro-CCHP system combined with an organic rankine cycle and vapor compression cycle. Energy Convers. Manage. 142, 374–384.

Chen, H., Pei, P., Song, M., 2015. Lifetime prediction and the economic lifetime of proton exchange membrane fuel cells. Appl. Energy 142, 154–163.

Corrêa, J.M., Farret, F.A., Canha, L.N., Simoes, M.G., 2004. An electrochemical-based fuel-cell model suitable for electrical engineering automation approach. IEEE Trans. Ind. Electron. 51 (5), 1103–1112.

Dhiman, G., Kumar, V., 2018. Emperor penguin optimizer: A bio-inspired algorithm for engineering problems. Knowl.-Based Syst. 159, 20–50.

Ebrahimian, Homayoun, et al., 2018. The price prediction for the energy market based on a new method. Econ. Res.-Ekon. Istraž. 31 (1), 313–337.

Eskandari Nasab, M., Maleksaeedi, I., Mohammadi, M., Ghadimi, N., 2014. A new multiobjective allocator of capacitor banks and distributed generations using a new investigated differential evolution. Complexity 19 (5), 40–54.

Firouz, Hosseini, Mansour, Ghadimi, Noradin, 2016. Optimal preventive maintenance policy for electric power distribution systems based on the fuzzy AHP methods. Complexity 21 (6), 70–88.

Ghadimi, N., Akbarimajd, A., Shayeghi, H., Abedinia, O., 2018. Two stage forecast engine with feature selection technique and improved meta-heuristic algorithm for electricity load forecasting. Energy 161, 130–142.

Ghadimi, N., Firouz, M.H., 2015. Short-term management of hydro-power systems based on uncertainty model in electricity markets. J. Power Technol. 95 (4), 265–272.

Ghadimi, N., Ojaroudi, M., 2014. A novel design of low power rectenna for wireless sensor and RFID applications. Wirel. Pers. Commun. 78 (2), 1177–1186.

Gollou, Rahimi, Abbas, Ghadimi, Noradin, 2017. A new feature selection and hybrid forecast engine for day-ahead price forecasting of electricity markets. J. Intell. Fuzzy Systems 32 (6), 4031–4045.

Gomes, G.F., da Cunha, S.S., Ancelotti, A.C., 2019. A sunflower optimization (SFO) algorithm applied to damage identification on laminated composite plates. Eng. Comput. 35 (2), 619–626.

Haghighi, M., Sharifhassan, F., 2016. Exergy analysis and optimization of a high temperature proton exchange membrane fuel cell using genetic algorithm. Case Stud. Therm. Eng. 8, 207–217.

Hamian, Melika, et al., 2018. A framework to expedite joint energy-reserve payment cost minimization using a custom-designed method based on mixed integer genetic algorithm. Eng. Appl. Artif. Intell. 72, 203–212.

Hosseini, H., Farsadi, M., Khalilpour, M., Razmjooy, N., 2011. Hybrid energy production system with PV array and wind turbine and pitch angle optimal control by genetic algorithm (GA).

Hosseini, H., Farsadi, M., Lak, A., Ghahramani, H., Razmjooy, N., 2012. A novel method using imperialist competitive algorithm (ICA) for controlling pitch angle in hybrid wind and PV array energy production system. Int. J. Tech. Phys. Prob. Eng. (IJTPE) (11), 145–152.

Infield, D., Freris, L., 2020. Renewable Energy in Power Systems. John Wiley & Sons.

Jain, M., Maurya, S., Rani, A., Singh, V., 2018. Owl search algorithm: a novel nature-inspired heuristic paradigm for global optimization. J. Intell. Fuzzy Systems 34 (3), 1573–1582.

Khodaei, Hossein, et al., 2018. Fuzzy-based heat and power hub models for cost-emission operation of an industrial consumer using compromise programming. Appl. Therm. Eng. 137, 395–405.

Kumar, Y., Singh, P.K., 2018. Improved cat swarm optimization algorithm for solving global optimization problems and its application to clustering. Appl. Intell. 48 (9), 2681–2697.

Leng, Hua, et al., 2018. A new wind power prediction method based on ridgelet transforms, hybrid feature selection and closed-loop forecasting. Adv. Eng. Inform. 36, 20–30.

Liu, Y., Lehnert, W., Janßen, H., Samsun, R.C., Stolten, D., 2016. A review of high-temperature polymer electrolyte membrane fuel-cell (HT-PEMFC)-based auxiliary power units for diesel-powered road vehicles. J. Power Sources 311, 91–102.

Liu, Yang, Wang, We, Ghadimi, Noradin, 2017. Electricity load forecasting by an improved forecast engine for building level consumers. Energy 139, 18–30.

Mascuch, J., Novotny, V., Vodicka, V., Spale, J., Zeleny, Z., 2020. Experimental development of a kilowatt-scale biomass fired micro–CHP unit based on ORC with rotary vane expander. Renew. Energy 147, 2882–2895.

Mehrfeld, P., et al., 2020. Dynamic evaluations of heat pump and micro combined heat and power systems using the hardware-in-the-loop approach. J. Build. Eng. 28, 101032.

Mirzapour, Farzaneh, et al., 2019. A new prediction model of battery and wind-solar output in hybrid power system. J. Ambient Intell. Humaniz. Comput. 10 (1), 77–87.

Namadchian, A., Ramezani, M., Razmjooy, N., 2016. A new meta-heuristic algorithm for optimization based on variance reduction of guassian distribution. Majlesi J. Electr. Eng. 10 (4), 49.

Nawaz, K., Shen, B., Elatar, A., Baxter, V., Abdelaziz, O., 2018. Performance optimization of CO2 heat pump water heater. Int. J. Refrig. 85, 213–228.

Park, C., Lee, H., Hwang, Y., Radermacher, R., 2015. Recent advances in vapor compression cycle technologies. Int. J. Refrig. 60, 118–134.

Razmjooy, N., Khalilpour, M., Ramezani, M., 2016. A new meta-heuristic optimization algorithm inspired by FIFA world cup competitions: Theory and its application in PID designing for AVR system. J. Control Autom. Elect. Syst. 27 (4), 419–440.

Razmjooy, N., Ramezani, M., 2014. An improved quantum evolutionary algorithm based on invasive weed optimization. Indian J. Sci. Res. 4 (2), 413–422.

Razmjooy, M., Ramezani, M., 2016. Model Order Reduction based on meta-heuristic optimization methods. In: 1st International Conference on New Research Achievements in Electrical and Computer Engineering Iran.

Romdhane, J., Louahlia, H., Marion, M., 2018. Dynamic modeling of an eco-neighborhood integrated micro-CHP based on PEMFC: Performance and economic analyses. Energy Build. 166, 93–108.

Ronaszegi, K., Fraga, E.S., Darr, J., Shearing, P.R., Brett, D.J., 2020. Application of photo-electrochemically generated hydrogen with fuel cell based micro-combined heat and power: A dynamic system modelling study. Molecules 25 (1), 123.

Rosli, R., et al., 2017. A review of high-temperature proton exchange membrane fuel cell (HT-PEMFC) system. Int. J. Hydrogen Energy 42 (14), 9293–9314.

Sahraie, H., Mirani, M.R., Ahmadi, M.H., Ashouri, M., 2015. Thermo-economic and thermodynamic analysis and optimization of a two-stage irreversible heat pump. Energy Convers. Manag. 99, 81–91.

Tian, M.-W., Yan, S.-R., Han, S.-Z., Nojavan, S., Jermsittiparsert, K., Razmjooy, N., 2019. New optimal design for a hybrid solar chimney, solid oxide electrolysis and fuel cell based on improved deer hunting optimization algorithm. J. Cleaner Prod. 119414.

Wang, G.-G., 2018. Moth search algorithm: a bio-inspired metaheuristic algorithm for global optimization problems. Memet. Comput. 10 (2), 151–164.

Wang, G.-G., Gao, X.-Z., Zenger, K., Coelho, L.d.S., 2018a. A novel metaheuristic algorithm inspired by rhino herd behavior. In: Proceedings of the 9th EUROSIM Congress on Modelling and Simulation, EUROSIM 2016, the 57th SIMS Conference on Simulation and Modelling SIMS 2016, Vol. 142. Linköping University Electronic Press, pp. 1026–1033.

Wang, D., Yu, B., Li, W., Shi, J., Chen, J., 2018b. Heating performance evaluation of a CO2 heat pump system for an electrical vehicle at cold ambient temperatures. Appl. Therm. Eng. 142, 656–664.

Yu, H., Huang, Z., Pan, Y., Long, W., 2020. Fuel Cell in Community Energy System. In: Guidelines for Community Energy Planning, Springer, pp. 423–454.

Yu, D., Wang, Y., Liu, H., Jermsittiparsert, K., Razmjooy, N., 2019. System identification of PEM fuel cells using an improved elman neural network and a new hybrid optimization algorithm. Energy Rep. 5, 1365–1374.